



**HAL**  
open science

## Variability and Remote Controls of the Warm-Water Halo and Taylor Cap at Maud Rise

Birte Gülk, Fabien Roquet, Alberto C. Naveira Garabato, Aditya Narayanan, clement rousset, Gurvan Madec

► **To cite this version:**

Birte Gülk, Fabien Roquet, Alberto C. Naveira Garabato, Aditya Narayanan, clement rousset, et al.. Variability and Remote Controls of the Warm-Water Halo and Taylor Cap at Maud Rise. *Journal of Geophysical Research. Oceans*, 2023, 128, 10.1029/2022JC019517 . insu-04188262

**HAL Id: insu-04188262**

**<https://insu.hal.science/insu-04188262v1>**

Submitted on 25 Aug 2023

**HAL** is a multi-disciplinary open access archive for the deposit and dissemination of scientific research documents, whether they are published or not. The documents may come from teaching and research institutions in France or abroad, or from public or private research centers.

L'archive ouverte pluridisciplinaire **HAL**, est destinée au dépôt et à la diffusion de documents scientifiques de niveau recherche, publiés ou non, émanant des établissements d'enseignement et de recherche français ou étrangers, des laboratoires publics ou privés.



Distributed under a Creative Commons Attribution - NonCommercial - NoDerivatives 4.0 International License

## Variability and Remote Controls of the Warm-Water Halo and Taylor Cap at Maud Rise



### Key Points:

- Interannual variability of the subsurface temperature maximum at Maud Rise is documented with observations
- Advection of anomalously cold and fresh deep waters from the Weddell Gyre into the Halo leads to a near-vanishing of the Taylor Cap in 2014
- Observed warming of the subsurface layer in the Taylor Cap due to eddy transport preceded the polynya opening in 2016–2017

### Supporting Information:

Supporting Information may be found in the online version of this article.

### Correspondence to:





B. Gülk,  
[birte.gulk@gu.se](mailto:birte.gulk@gu.se)

### Citation:

Gülk, B., Roquet, F., Naveira Garabato, A. C., Narayanan, A., Rousset, C., & Madec, G. (2023). Variability and remote controls of the warm-water Halo and Taylor Cap at Maud Rise. *Journal of Geophysical Research: Oceans*, 128, e2022JC019517. <https://doi.org/10.1029/2022JC019517>

Received 28 NOV 2022

Accepted 21 JUN 2023

Birte Gülk<sup>1</sup> , Fabien Roquet<sup>1</sup> , Alberto C. Naveira Garabato<sup>2</sup> , Aditya Narayanan<sup>1</sup> , Clément Rousset<sup>3</sup>, and Guran Madec<sup>3</sup>

<sup>1</sup>Department of Marine Science, University of Gothenburg, Göteborg, Sweden, <sup>2</sup>Ocean and Earth Science, University of Southampton, National Oceanography Centre, Southampton, UK, <sup>3</sup>LOCEAN-IPSL, Laboratoire d'Océanographie et du Climat: Expérimentation et Approches Numériques, Sorbonne Université/CNRS/IRD/MNH, Paris, France

**Abstract** The region of Maud Rise, a seamount in the Weddell Sea, is known for the occurrence of irregular polynya openings during the winter months. Hydrographic observations have shown the presence of a warmer water mass below the mixed layer along the seamount's flanks, commonly termed the *warm-water Halo*, surrounding a colder region above the rise, the *Taylor Cap*. Here we use two observational data sets, an eddy-permitting reanalysis product and regional high-resolution simulations, to investigate the interannual variability of the Halo and Taylor Cap for the period 2007–2022. Observations include novel hydrographic profiles obtained in the Maud Rise area in January 2022, during the first SO-CHIC cruise. It is demonstrated that the temperature of deep waters around Maud Rise exhibits strong interannual variability within the Halo and Taylor Cap, occasionally to such an extent that the two features become indistinguishable. A warming of deep waters by as much as 0.8°C is observed in the Taylor Cap during the years preceding the opening of a polynya in 2016 and 2017, starting in 2011. By analyzing regional simulations, we show that most of the observed variability in the Halo is forced remotely by advection of deep waters from the Weddell Gyre into the region surrounding Maud Rise. Our highest-resolution simulation indicates that mesoscale eddies subsequently transfer the properties of the Halo's deep waters onto the Taylor Cap. The eddies responsible for such transfer originate in an abrupt retroflection along the inner flank of the Halo.

**Plain Language Summary** A polynya is an opening within the sea ice cover during winter. In the Weddell Sea, polynyas occur irregularly and often emerge close to a seamount, Maud Rise. This topographic obstacle disturbs the local circulation of the Weddell Gyre and leads to the formation of two local permanent features: a Taylor Cap on top of the seamount, which is mainly an isolated water mass; and surrounding this, a warm-water Halo, located along the flanks of Maud Rise. In this study, we use observational and model analyses to show the changes in the temperature of regional water masses on a timescale of years, and to identify the drivers of these changes. The properties of the warm-water Halo are controlled by the advection of deep waters along the south-eastern rim of the Weddell Gyre. These waters are partly mixed into the Taylor Cap by eddies, thereby preconditioning the water column for deep convection. In the years preceding the opening of a polynya in 2016–2017, we document a warming trend in the Taylor Cap, starting in 2011.

## 1. Introduction

In the austral winters of 1974–1976, an opening of the sea ice was observed by satellites in the Weddell Sea: the Weddell Polynya (Gordon, 1982). Since then smaller and short-lived openings (termed Maud Rise Polynyas (Comiso & Gordon, 1987)) have been detected (Campbell et al., 2019). All polynyas had in common that they occurred in the vicinity of Maud Rise, a seamount located at 2.5°E, 65°S and rising from 5,000 to 1,800 m (Figure 1). The most recent Maud Rise Polynyas were observed in 2016 and 2017. A range of theories and hypotheses for polynya formation have been put forward, and are reviewed in the latter part of this section. Hydrographic observations around Maud Rise reveal the presence of a flow pattern that is similar to a Taylor Column on top of the seamount, surrounded by a warmer subsurface water mass (Gordon & Huber, 1990).

A Taylor Column results from the interaction of a two-dimensional barotropic flow with a topographic obstacle. Its dynamics were first explained by Taylor (1923) and Proudman (1916) in the Taylor-Proudman theorem. The theorem describes how fluid parcels in a barotropic, frictionless and steady flow moving on a horizontal plane, cannot leave their plane in the vertical direction; this implies that the fluid parcels are not able to

© 2023 The Authors.

This is an open access article under the terms of the [Creative Commons Attribution-NonCommercial License](https://creativecommons.org/licenses/by/4.0/), which permits use, distribution and reproduction in any medium, provided the original work is properly cited and is not used for commercial purposes.

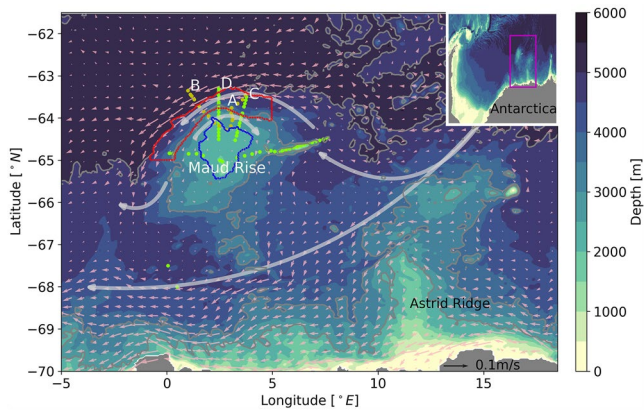


**Figure 1.** Topography of the domain of Maud12 and Maud36, with the CTD casts (January 2022, green dots) and an instrumented seal transect identified in EN4.2.2 (May 2013, yellow dots). The gray arrows schematize the flow of the southern limb of the Weddell Gyre, supported by the depth-averaged mean flow derived from GLORYS12 for the period 2007–2017 (pink arrows). The inlay shows the Weddell Sea and the zoomed-in area (purple box).

flow over the obstacle. Due to the topographically-induced compression/stretching of the water column upstream/downstream of the obstacle, the fluid parcels are forced to go around it, such that a stagnant water column forms on top of the obstacle. The presence of stratification reduces this topographic constraint, and instead a Taylor Cap develops. Taylor Caps are bottom-trapped and sensitive to both the stratification and inflow intensity (Chapman & Haidvogel, 1992). Further, they may host substantial vertical motions and a net vertical mass transport (Sévellec et al., 2015).

The observed flow pattern around Maud Rise leading to the local emergence of a Taylor Cap is associated with the wind-driven Weddell Gyre. The Gyre bifurcates into two jets at Maud Rise (Leach et al., 2011): a stronger one along the northern flank (transporting 14 Sv,  $1 \text{ Sv} = 10^6 \text{ m}^3 \text{ s}^{-1}$ ) and a weaker one along the southern flank (4 Sv) (Schröder & Fahrbach, 1999) (schematized in Figure 1). South of the northern jet, an eastward return current, termed the retroflexion current, is found (Cisewski et al., 2011). The Gyre conveys Warm Deep Water (WDW), originating from Circumpolar Deep Water (CDW) in the Antarctic Circumpolar Current (ACC), toward and along the flanks of Maud Rise (Reeve et al., 2019; Schröder & Fahrbach, 1999). As WDW is a relatively warm ( $0^\circ\text{C} \leq \theta \leq 1.5^\circ\text{C}$ ) and saline water mass (Ryan et al., 2016), it provides the main heat source to the Weddell Gyre besides

solar radiation (Reeve et al., 2019). The Gyre's flow along the northern flank of Maud Rise is visible in observations as a zone with a high subsurface temperature maximum; this is the warm-water Halo (De Steur et al., 2007; Gordon & Huber, 1990; Muench et al., 2001).

Previous observations in 1986, 1994, 2005 and 2019/20 (De Steur et al., 2007; Gordon & Huber, 1990; Mohrmann et al., 2022; Muench et al., 2001) consistently identified the Taylor Cap by a temperature maximum below the mixed layer depth (MLD) of approximately  $0.4^\circ\text{C}$  on top of Maud Rise; and the warm-water Halo by maximum temperatures exceeding  $1^\circ\text{C}$  along the flanks of the seamount. The warm-water Halo is less marked along the southern flank of Maud Rise, and does not fully encircle the seamount. Substantial spatio-temporal variability in the width and depth of the Halo, and of its associated thermocline and halocline, has been observed (De Steur et al., 2007; Muench et al., 2001), but evidence of variability has been limited due to the scarcity of long-term observations in the Maud Rise area. Such modest knowledge of the Halo's variability stands in contrast with its potentially important role in moderating sea-ice concentration around the Rise (Lindsay et al., 2008), and in influencing the emergence of open-ocean polynyas. Thus, systematically documenting the spatio-temporal variability of the Halo is imperative to elucidate the extent to, and manner in which, it may control Taylor Cap properties and the formation of Maud Rise Polynyas.

A range of atmospheric, oceanic and coupled atmospheric-oceanic processes have been recently put forward as being instrumental in opening of a Maud Rise Polynya. The suggested atmospheric processes include atmospheric rivers (Francis et al., 2020) and severe storms in combination with upper-ocean preconditioning by salinity (Campbell et al., 2019). Francis et al. (2020) proposed that, in 1973 and 2017, atmospheric rivers preconditioned the sea ice and opened a polynya via cyclonic wind-driven sea-ice divergence. Their hypothesis suggested that atmospheric rivers may transport moisture and heat into the Maud Rise region, and induce a warming that results in sea-ice melting. However, since sea-ice melting enhances stratification, much uncertainty persists around the mechanism governing polynya opening. Severe storms, as suggested by Campbell et al. (2019), can cause sea-ice divergence and also enhance turbulent vertical mixing in the upper water column. Sea-ice divergence leads to rapid ice growth and brine rejection, adding salt to the mixed layer; concurrently, salt and heat are brought to the mixed layer by turbulent vertical mixing. The additional heat then melts the sea ice that was just formed in association with sea-ice divergence, and the stabilizing effect of such meltwater acts to suppress further turbulent entrainment. The effect of (de-)entrainment of salt on upper-ocean stability can be expressed by the “salt deficit” (Martinson, 1990), which describes the necessary amount of additional salt by brine rejection from sea-ice formation required to destabilize the upper water column. In the case of a preconditioned mixed layer with an increased salinity, as was observed by Campbell et al. (2019), the “salt deficit” is modest and the likelihood of triggering deep convection is increased. Alternatively, solely oceanic processes have been proposed to drive polynya emergence. Such processes include the interaction of the Weddell Gyre with the flanks of Maud Rise (Cheon

& Gordon, 2019), the shedding of mesoscale eddies at these flanks (Holland, 2001), the advection of high surface salinity into the area around the Rise (Kurtakoti et al., 2018), and processes contingent on the non-linear equation of state, such as thermobaricity (Akitomo, 2006; McPhee, 2000) and thermobaric cabbelling (Harcourt, 2005). Cheon and Gordon (2019) suggested that, in 2017, an intensified Weddell Gyre enhanced eddy formation at the flanks of Maud Rise, which promoted upwelling of heat and exerted a divergent stress on the sea ice. The Gyre was indicated to have been spun-up by an intensified cyclonic wind stress curl over the Weddell Sea, linked to strengthened Southern Hemisphere westerlies. Holland (2001) proposed that eddies shed at the Rise's northeastern flank transmit divergent Ekman stresses onto the ice, leading to an opening of the polynya. In turn, Kurtakoti et al. (2018) used a high-resolution Earth-system model to argue that polynya formation is usually preceded by a build-up of a large heat reservoir at depth, and triggered by vertical mixing driven by an energized Weddell Gyre and the advection of high surface salinity anomalies from the east. Both observational and modeling investigations have shown that the flanks of Maud Rise are susceptible to thermobaricity (Akitomo, 2006; McPhee, 2000), with Harcourt (2005) suggesting that instabilities may develop locally due to a combination of thermobaricity and cabbelling.

A point of agreement of most past works concerns the requirement of a substantial amount of heat below the mixed layer to trigger deep convection and sea-ice opening around Maud Rise. The most immediate source of such heat is provided by the warm-water Halo and Taylor Cap system. Motivated by this potentially instrumental role in Maud Rise Polynya formation, here we document the interannual variability of the warm-water Halo and Taylor Cap during the period 2007–2022, covering the most recent polynya openings, and assess its controlling mechanisms in order to elucidate the features' origins and interplay. Specifically, we investigate whether the variability in the area of the Rise is driven by local processes specific to Maud Rise, or remote processes acting over larger scales such as for example, the Weddell Gyre. Our analysis exploits: an observational data set integrating EN4.2.2 (Good et al., 2013) and a set of CTD sections acquired by the SO-CHIC programme in 2022 (Sallée et al., 2023); a global assimilated NEMO (Nucleus for European Modelling of the Ocean) model, GLORYS12 (Lellouche et al., 2021); and two regional NEMO ocean model configurations, Maud12 and Maud36, to elucidate fine-scale ice-ocean processes and their role in regional water-mass changes. Our methods and data sets are presented in Section 2, and our results in Section 3. The interpretation of these results is discussed, and conclusions are drawn, in Section 4.

## 2. Methods and Data

### 2.1. Methods

For our analysis, we define the Taylor Cap as the area over Maud Rise with bathymetry shallower than 2,500 m (Figure 1, blue-encircled area), and the Halo as the area around the Rise's northern flank in water depth of 3,500–5,000 m (north of 65°S and west of 5°E; Figure 1, red-encircled area). These definitions reflect the Taylor Cap's topographically bounded nature, and the delineation of the Halo's core as a quasi-stationary feature by previous observational campaigns (De Steur et al., 2007; Gordon & Huber, 1990; Muench et al., 2001). In all data sets, we define MLD as the depth at which the surface-referenced potential density exceeds density at 10 m by  $\Delta\sigma_0 = 0.01 \text{ kg m}^{-3}$  which was previously used in the Southern Ocean for example, by Rodgers et al. (2014). In the observations, this estimate is done during the post-processing of the data, and in the models the computation is done online. The maximum temperature below the MLD,  $T_{\text{max}}$ , is calculated in both observations and models. The observational  $T_{\text{max}}$  values are insensitive to the density threshold for the MLD.

Our analysis is grounded on the computation of a heat budget for the Taylor Cap, with the goal of elucidating the processes controlling the variability of the Cap's heat content. The heat budget is constructed for three ranges: the surface layer (<200 m), the subsurface layer (200–1,000 m) and the deep layer (>1,000 m). The surface layer is selected to capture the seasonal cycle in upper-ocean properties associated with sea-ice growth and melt. The subsurface layer encompasses the depth range in which  $T_{\text{max}}$  is present, and thereby enables estimation of vertical exchanges of heat between waters around the  $T_{\text{max}}$  and other layers. The deep layer includes all waters below 1,000 m, which are expected to be renewed more sluggishly in the area (Campbell et al., 2019).

The heat budget involves three terms: the temporal change of the heat content, the advective heat flux, and the surface heat flux. The heat content,  $H$ , is defined as

$$H = \rho_0 c_p \int_V \theta dV \quad , \quad (1)$$

where  $\rho_0$  is the density of seawater,  $c_p$  the specific heat of seawater, and temperature  $\theta$  is integrated within each layer's volume,  $V$ . Here,  $\rho_0 = 1,026 \text{ kg m}^{-3}$  and  $c_p = 4,000 \text{ J kg}^{-1} \text{ K}^{-1}$  are assumed to be constant. The advective heat flux,  $F^\theta$ , is the combined horizontal ( $F_h^\theta$ ) and vertical ( $F_v^\theta$ ) heat flux, and is given by:

$$F^\theta = \rho_0 c_p \nabla \cdot (\vec{U} \theta) , \quad (2)$$

where  $\vec{U}$  is the 3-d transport through the boundaries of the layer's volume. The eddy contribution to the advective flux is also computed, by using the respective deviations,  $\vec{U}'$  and  $\theta'$ , from the time-mean  $\vec{U}$  and  $\theta$  (calculated from the full simulations) in expression 2. The heat budget of each layer may then be written as

$$\frac{\partial H}{\partial t} = \left( \int_A Q_{net} dA + F^\theta \right) + R . \quad (3)$$

Here,  $Q_{net}$  is the surface heat flux, which is provided by the model and contains the short- and long-wave radiation fluxes, the sensible and latent heat fluxes, and the conductive heat flux induced by sea ice.  $Q_{net}$  is zero for the subsurface and deep layers.  $R$  denotes the residual, which accounts for diffusion of heat.

## 2.2. Observations

We consider the EN4.2.2 data set (Good et al., 2013), which compiles hydrographic profiles throughout the global ocean, acquired via various observational systems such as Argo, ASBO, GTSP, World Ocean Database 2018, and MEOP (McMahon et al., 2021). Duplicate profiles are excluded by the processing of the data (Good et al., 2013). In this study, we only use profiles that had temperature and salinity available and reached a depth of at least 300 m during the period January 2007–May 2022, and extracted the Maud Rise region ( $5^\circ\text{W}$ – $19^\circ\text{E}$  and  $62^\circ\text{S}$ – $69^\circ\text{S}$ ; Figure 1, purple box; the positions of the profiles can be found in Figure S1 in Supporting Information S1). In what follows, data profiles with a salinity lower than  $32 \text{ g kg}^{-1}$  or a temperature exceeding  $10^\circ\text{C}$  at 10 m depth are excluded. This yields a total of 6,732 profiles, of which 278 are in the Taylor Cap and 211 in the Halo. In our processing of the data, we linearly re-grid all profiles onto a regular vertical grid with spacing of 5 m.

Besides the EN4.2.2 data set, we include 58 CTD casts measured during 8–15 January 2022 as part of the first SO-CHIC cruise on the S.A. Agulhas II, in the Maud Rise region (Ward et al., 2022). These CTD casts span two sections across the northern flank of Maud Rise, and a further two sections extending from the center of Maud Rise to the east and west (Figure 1, green dots). All casts reached a depth of at least 1,000 m. The data are processed in 1 m vertical intervals.

## 2.3. GLORYS12

GLORYS12V1 is a global NEMO (Madec & NEMO System Team, 2019) configuration assimilated with observations, which provides daily data from 1 January 1993 to 31 May 2020 on a  $1/12^\circ$  horizontal Mercator grid with 50 vertical levels (Lellouche et al., 2021). The initial state of temperature and salinity is derived from EN4.2.0 (Good et al., 2013). The surface is forced with atmospheric state variables derived from ERA-Interim and ERA5. The observations used for the data assimilation are along-track altimeter data, satellite sea-surface temperature and sea-ice concentration, and in situ temperature and salinity profiles from Lagrangian platforms and ship-based measurements. GLORYS12 is used to provide an overview of processes operating in the study region when no observations are available. However, assimilation of data introduces non-conservative perturbations, making the product unsuitable for heat or salt budgets. In particular, years 2018–2020 are unreliable due to ingestion of bad-quality data, so we will focus solely on the period 2007–2017 in this study.

## 2.4. Maud12 and Maud36

Maud12 and Maud36 are regional NEMO configurations with ocean and ice components (Madec & NEMO System Team, 2019; NEMO Sea Ice Working Group, 2018). The configurations cover the region from  $5^\circ\text{W}$  to  $19.5^\circ\text{E}$  and  $61.5^\circ\text{S}$  to  $70.5^\circ\text{S}$  (Figure 1). They have 50 vertical levels and only differ in their horizontal resolution, which is  $1^\circ/12^\circ$  for Maud12 and  $1/36^\circ$  for Maud36, resulting in respective horizontal resolutions of 3.9 and 1.3 km at  $65^\circ\text{S}$ . Maud12 runs from 1 January 2007 to 19 May 2020, and provides daily output. Years 2018–2020



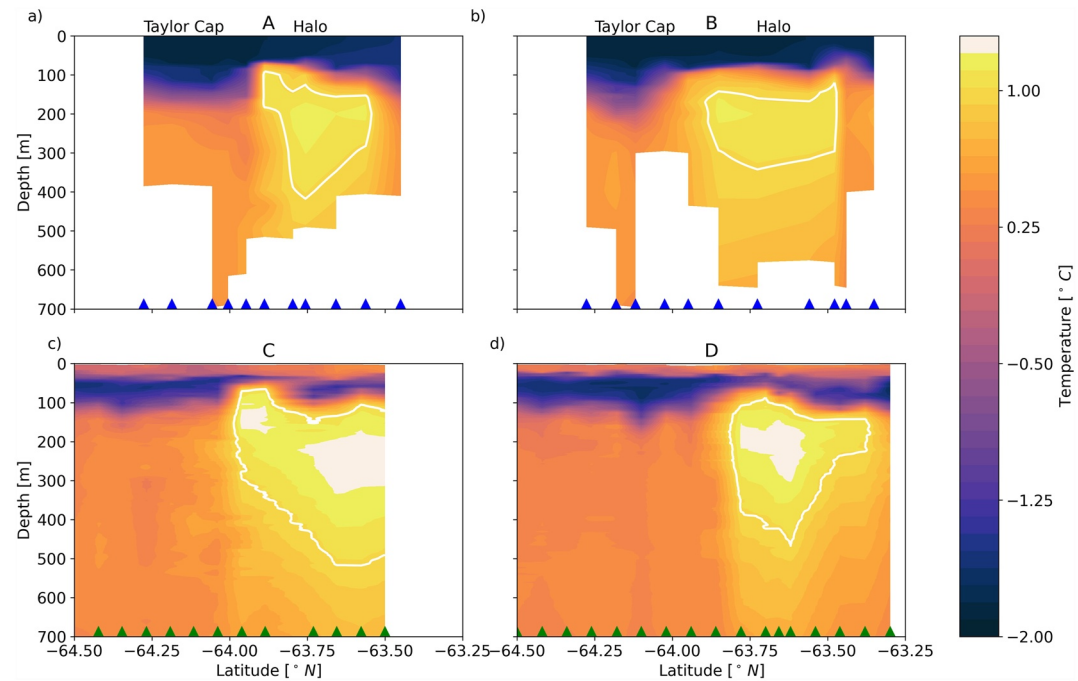


**Figure 2.** Temperature sections acquired by an instrumented seal in May 2013 (a and b) and via CTD casts in January 2022 (c and d) with 1°C isotherm (white contours). Section labels and markers refer to Figure 1.

were excluded, as GLORYS12V1 was found to be unreliable in that period due to the ingestion of erroneous in situ data. The bathymetry is derived from GEBCO (GEBCO Compilation Group, 2022). The lateral boundary forcing and initial state are taken from GLORYS12V1. The surface is forced by JRA55-do version 1.5 (Tsujino et al., 2018). By developing Maud12, we gain insight into physical processes without the effects of data assimilation, with a comparable resolution as GLORYS12. Maud12 can readily be used for process studies thanks to its small domain size and fast spin-up period. Further, it is used as reference for Maud36, which seeks to assess the importance of finer-scale dynamics around Maud Rise. Maud36 simulates the period from 1 January 2007 to 31 December 2017. The rationale for this shorter simulation is that it excludes the post-2018 period of unreliable GLORYS12 output. Owing to its higher horizontal resolution, Maud36 resolves mesoscale variability and provides clearer insight into the impacts of eddies on the local stratification and circulation features around Maud Rise. As will be shown, Maud12 and Maud36 failed to develop a polynya event in 2016 and 2017, so they diverge from observations from 2016 onwards and cannot be used to study the occurrence of deep convection at that time.

### 3. Results

#### 3.1. Temperature Variability

##### 3.1.1. Observations

In May 2013 an instrumented elephant seal crossed the northern flank of Maud Rise, in the same region as the northern SO-CHIC CTD transects in January 2022 (Figure 1, yellow and green dots). These sections (Figure 2) have similar starting positions and comparable orientations, and cross the Halo twice. Temperature along the sections reveal the core of the Halo ( $\theta > 1.0^{\circ}\text{C}$ , bright yellow areas in Figure 2), as well as temperature fronts on approaching the summit of Maud Rise. The depth of the  $T_{\text{max}}$  core nearly doubles between the two periods from 200 to 400 m. The thickness of the warm core is greater in 2022 than in 2013, hinting a substantial interannual variability.

Inspection of the  $T_{\text{max}}$  across all EN4 profiles and CTD casts in the period 2007–2022 reveals the position of the colder Taylor Cap and the warm-water Halo surrounding Maud Rise (Figure 3). The highest  $T_{\text{max}}$  values are found to the east and along the northern flank of Maud Rise. The warmer  $T_{\text{max}}$  is approximately bounded by the 3,500 m and 5,000 m isobaths. On the western side of Maud Rise, where the topographic slope relaxes, a slightly cooler

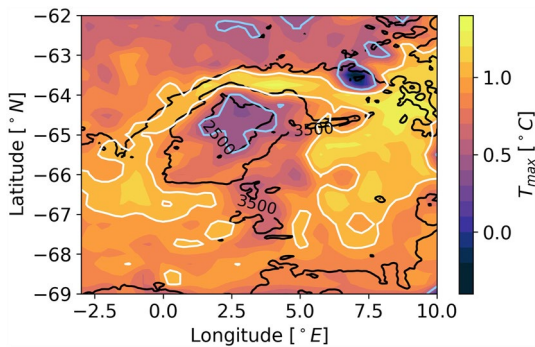


**Figure 3.**  $T_{\max}$  of observations acquired during the period 2007–2022, gridded according to a radial basis function interpolation in longitude and latitude, with the 2,500, 3,500, and 5,000 m isobaths (black lines) and 0.5°C (lightblue) and 1.0°C (white) isotherms. Stars indicate positions used in Figure 6. The positions of profiles considered in this analysis are shown in Figure S1 in Supporting Information S1.

$T_{\max}$  is found than in the northern flank. North of the Halo, in areas deeper than 5,000 m, the  $T_{\max}$  is cooler.

Pooling together all profiles into the areas of the Halo and Taylor Cap (red- and blue-encircled areas, respectively, in Figure 1) enables construction of a time series of the  $T_{\max}$  in each region (Figures 4a and 4b, black dots). The  $T_{\max}$  in the Halo is spread over a temperature range of 0.1°C–1.3°C, with a high number of profiles showing temperatures exceeding 1.0°C. The observed  $T_{\max}$  in the Halo in 2008 is mainly around 1.1°C, and the few available profiles in years 2009–2010 indicate a decrease of  $T_{\max}$ . In 2018, for which 35 profiles are available,  $T_{\max}$  is around 1.1°C again, and in 2020–2022  $T_{\max}$  reaches 1.2°C. In the Taylor Cap, profiles in 2007–2009 exhibit a  $T_{\max}$  of approximately 0.4°C. After a substantial observational gap, a  $T_{\max}$  of 0.9°C is observed in 2015; this is the maximum found in the entire 2007–2022 period. The observations then show a reduction in  $T_{\max}$  following the peak  $T_{\max}$  values. From 2018 onward, the majority of profiles exhibit a  $T_{\max}$  returning back to 0.4°C.

The observational gap makes it difficult to evaluate the causes of the temperature change in the Taylor Cap with any confidence; for example, we cannot reliably assess if the temperature change between 2010 and 2015 occurs abruptly or over several years. This motivates us to examine the model outputs of GLORYS12 (which is assimilated with the measurement profiles considered here), and Maud12 and Maud36 (without data assimilation), in the next section.

### 3.1.2. Observations Versus Models

The observed  $T_{\max}$  data are compared to the horizontal averages estimated in GLORYS12, Maud12 and Maud36 for the Halo and Taylor Cap (Figures 4a and 4b). In the Halo, a warming of  $T_{\max}$  until 2013 is found in all models,

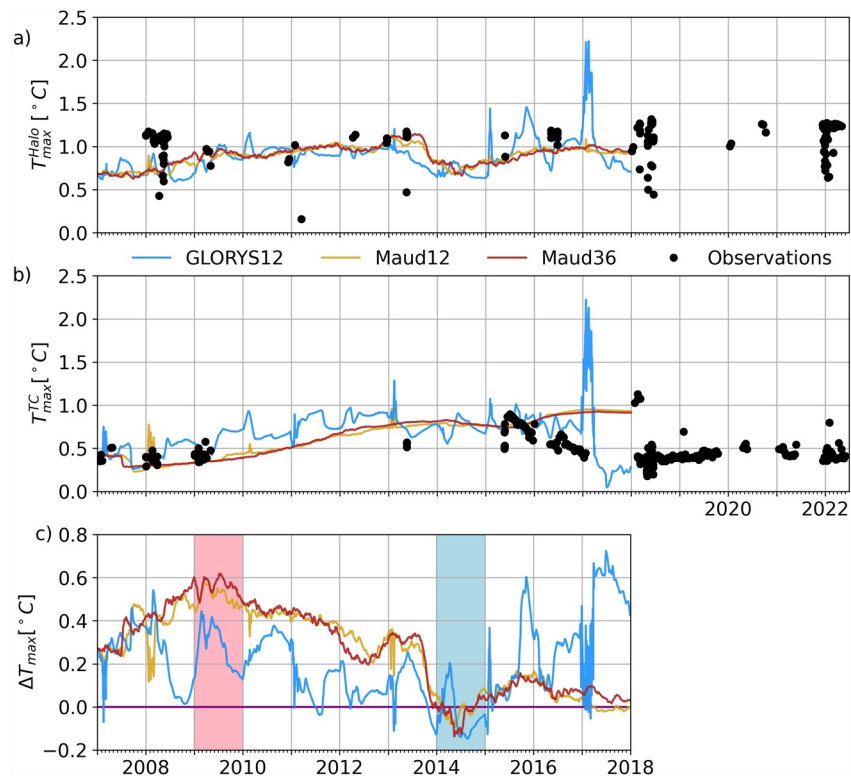


**Figure 4.**  $T_{\max}$  for GLORYS12 (blue), Maud12 (yellow), Maud36 (red) and the observations (black dots) in (a) the Halo, and (b) the Taylor Cap. (c) Difference between  $T_{\max}$  in the Halo and Taylor Cap in the models. The purple line is 0°C. The year with the largest/smallest difference are shaded with red/blue.

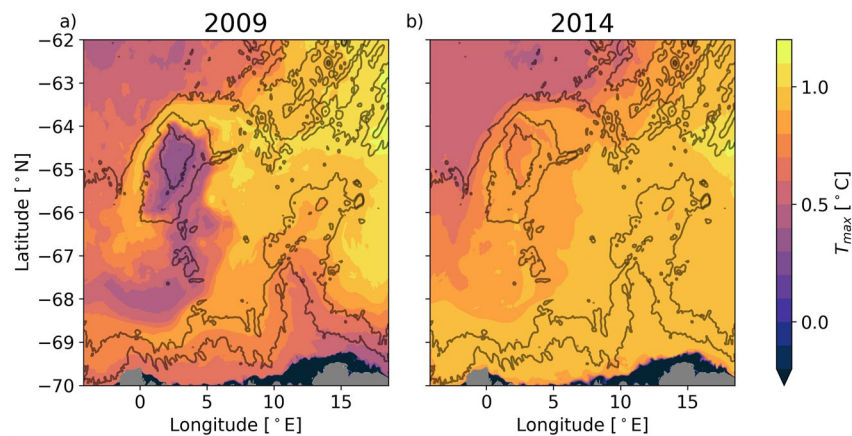


**Figure 5.** Spatial distribution of the averaged  $T_{\max}$  in Maud36 in (a) 2009 and (b) 2014.

followed by a rapid cooling in 2013–2014. Maud12 and Maud36 display warming until 2018. While this warming is also found in GLORYS12, there is a sudden change in  $T_{\max}$  afterward. The  $T_{\max}$  values estimated from Maud12 and Maud36 are within the range of the observations, and are similar to each other. The highest  $T_{\max}$  value in GLORYS12 reach up to 2°C in 2017. In the Taylor Cap, the  $T_{\max}$  in the models is around 0.5°C in the period 2007–2009 (Figure 4b). Then the models show a continuous warming until 2015, at which time the models'  $T_{\max}$  values agree with those in the observations. After 2015, the models'  $T_{\max}$  disagree with one another. GLORYS12 cools down from 0.9°C to 0.5°C in 2017 following opening of the polynya, in agreement with observations. At this point, GLORYS12 exhibits an abrupt change in  $T_{\max}$ , with large fluctuations of more than 1°C within a couple of months. This cooling is, however, not observed in Maud12 and Maud36, likely due to the absence of a polynya event in 2016 and 2017 in these simulations. The difference in  $T_{\max}$  between the Halo and the Taylor Cap (Figure 4c) denotes substantial interannual variability, with a marked difference ranging from 0.3°C to 0.6°C prior to 2014. In 2014, the  $T_{\max}$  of both features abruptly becomes comparable, and the Taylor Cap is even warmer than the Halo during a brief period (blue shaded area in Figure 4c) - such that the Taylor Cap and Halo essentially become indistinguishable (Figure 5).

To understand what drives the variability of  $T_{\max}$  across Maud Rise, we next investigate the water mass structure within the upper 1,300 m in the Halo (Figure 1; red-encircled area) and in the Taylor Cap (Figure 1; blue-encircled area) in the context of the evolving sea-ice concentration in GLORYS12 and Maud36 (Figure 6).

### 3.2. Vertical Variability

In GLORYS12, the vertical structure of the Halo (Figure 6a) exhibits an overall warming tendency up until 2013, followed by a sharp reduction in density (apparent as a deepening of the  $\sigma_0 = 27.67 \text{ kg m}^{-3}$  isopycnal (black dotted line in Figure 6a)). This density decrease is concurrent to reduced temperatures and salinities (not shown). In 2014, a brief period with deep mixing down to 800 m is found in parts of the Halo; this leads to a cooling of the water column. This deep mixing could be an artifact of the assimilation procedure. Such brief deep-convection event, and the associated occurrence of a cold, fresh water mass below the winter mixed layer, result in a reduction of  $T_{\max}$  at the end of 2013 and beginning of 2014 (Figure 4). In 2015 and 2016, a warm layer with temperatures exceeding 1.0°C and a thickness greater than 200 m is present in the Halo; this is the period in which the peak  $T_{\max}$  occurs (Figure 4). From 2017 onwards, the warm layer vanishes. During the entire 2007–2016 period, the sea-ice concentration undergoes a standard seasonal cycle. In 2017, the sea-ice concentration deviates from the patterns of the previous years and decreases in the middle of the winter.

In Maud36, the vertical temperature structure in the Halo (Figure 6b) shows similar temperature patterns until 2013, and also a significant change in the upper 1,300 m in 2013–2014, as in GLORYS12. The 2013–2014 change results from the appearance of a fresher and more stable water mass (see Figures S3a and S3b in Supporting Information S1) and not a deep convection event (see Figure S2 in Supporting Information S1). After 2015, the temperature patterns diverge, with GLORYS12 showing a substantial warming at depths of 150–500 m (with temperatures exceeding 1.5°C), and Maud36 simulating cooler temperatures around 1.0°C. The temperature



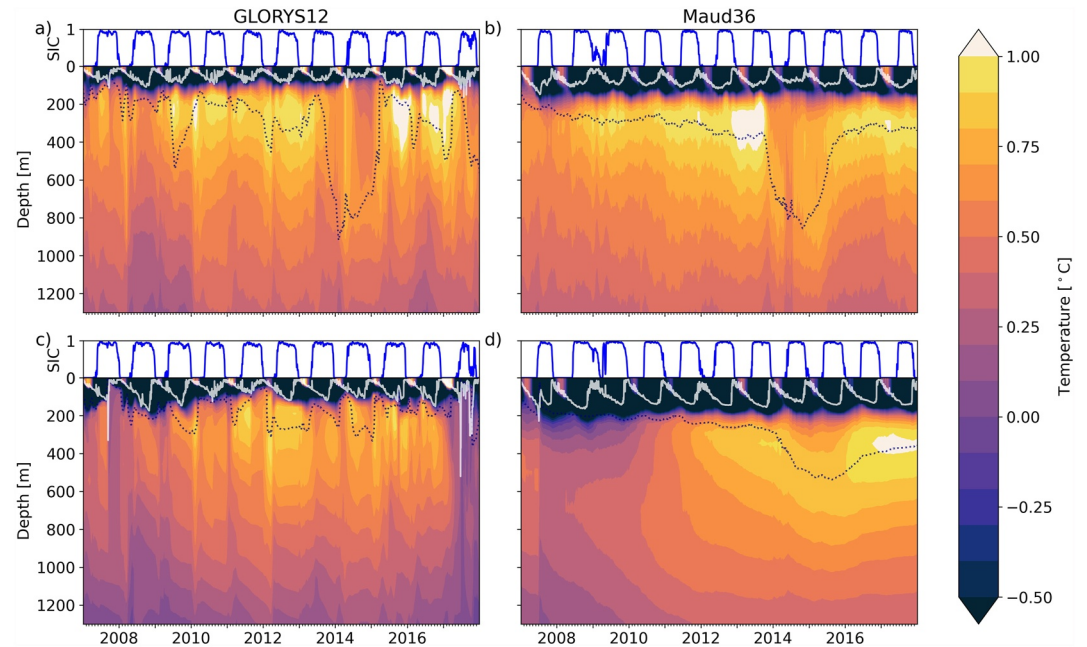


**Figure 6.** Time series of spatial-mean temperature in the Halo (upper row) and Taylor Cap (lower row) for GLORYS12 (a and c) and Maud36 (b and d), overlaid with the mixed layer depth (white line) and the  $\sigma_0$ -isopycnal of  $27.67 \text{ kg m}^{-3}$  (black dotted line). Blue lines in the upper bar of each plot indicate the sea-ice concentration at the respective location.

structure in Maud36 after 2015 resembles that found between 2008 and 2011. The modeled pattern for Maud36 reproduces well the computed  $T_{\max}$  in Figure 4, with an increase until 2013, a cooling in 2014–2015, and a subsequent warming.

In GLORYS12, in the Taylor Cap (Figure 6c), a deep convection event reaching down to 750 m takes place in late 2007, cooling the water column. Subsequently, a water column warming occurs until 2015. The water column then remains in this warm state until 2017, when a long, deep convection event induces strong water column cooling. While the brief convection event in 2007 occurred in conjunction with a closed sea-ice cover, the convection events in 2016 and 2017 were associated with polynya openings.

In Maud36, in the Taylor Cap (Figure 6d), the deep convection event in late 2007 and its cooling of the water column is reproduced, similarly to GLORYS12. This deep convection event freshens and destabilizes the water column (see Figures S3c and S3d in Supporting Information S1). After this cooling, the water column in Maud36 undergoes a warming trend over the 2009–2017 period. This warming trend concurs with the development of  $T_{\max}$  (Figure 4). In 2014, a sharp density reduction occurs, indicated by the  $27.67 \text{ kg m}^{-3}$ -isopycnal (black dotted line). A shoaling of this isopycnal follows in 2016. This density signal mimics that found in the Halo, with a sudden change. This indicates the existence of a dynamical connection between the Halo and the Taylor Cap. Maud36 and GLORYS12 show similarities in 2007 and 2008, after then the temperature patterns in the Taylor Cap disagree. Maud36 is unable to reproduce the deep convection events and polynya openings in 2016 and 2017, which cool the water column locally. In turn, GLORYS12, unlike Maud36, reveals no obvious dynamical relation between the Halo and Taylor Cap.

From Figure 6 we can conclude that the cooling in the Taylor Cap is a result of deep convection events, but the origin of the warming tendency is unclear. Since such warming is similar between the models before the polynya opens, we will analyze the dynamics of the Halo and Taylor Cap by focusing on the Maud36 simulation, which provides superior resolution of likely important fine-scale processes. Further, Maud36 is not negatively affected by data assimilation, which is believed to be responsible for the unrealistic sudden temperature changes in Figure 4.

As indicated by the spatial mean of  $T_{\max}$  (Figure 5) and the evolution of the upper-ocean temperature (Figure 6), substantially different spatial distributions of temperature occur in 2009 and 2014. To explore this difference, we

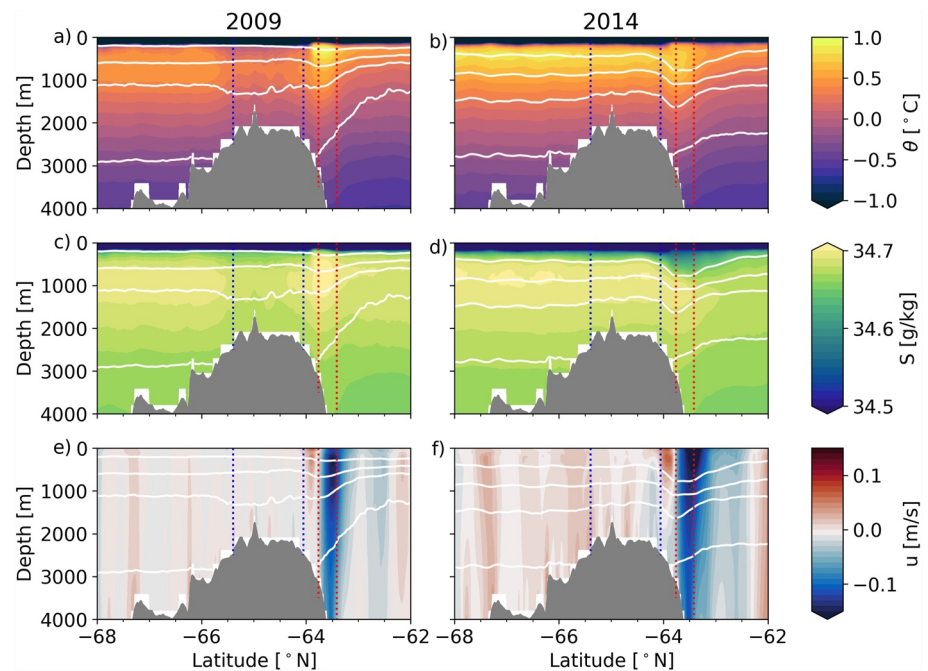


**Figure 7.** Time-mean temperature, salinity, and zonal velocity sections along  $2.4^{\circ}\text{E}$ , with isopycnals (white lines), for 2009 and 2014 in Maud36. Blue/red dotted lines indicate the boundaries of the Taylor Cap/Halo in this section.

examine a section of temperature, salinity and zonal velocity along  $2.4^{\circ}\text{E}$  across Maud Rise for 2009 and 2014 in Maud36 (Figure 7). The temperature and salinity sections for 2009 indicate the presence of a warm and salty layer above 1,000 m, the WDW, in the Taylor Cap. Above this layer, isotherms and isohalines are depressed, whereas they are domed below the layer (Figures 7a and 7c). The warm and salty layer is thinner, cooler and fresher over Maud Rise than on the Rise's flanks. The Halo is apparent on the northern flank of Maud Rise at  $63.5^{\circ}\text{S}$ , with a warm and saline core below the winter mixed layer. The Halo is characterized by high westward velocities (Figure 7e), while the Taylor Cap exhibits weak flow. Between the Taylor Cap and Halo, the eastward retroflection current is present in the upper 1,500 m. While the circulation patterns found in 2009 resemble those presented by (Cisewski et al., 2011), the circulation patterns in 2014 differ strongly. The previously domed isotherms and isohalines in the Taylor Cap are now flattened, and the temperature and salinity properties within the Cap are similar to those onshore of Maud Rise (Figures 7b and 7d). Along this section, the Taylor Cap has seemingly lost its distinct colder temperature and lower salinity properties. In the location, where the Halo's warm and saline waters were found in 2009, a colder and fresher water mass is present in 2014. These observed hydrographic changes are accompanied by a major shift in the zonal velocity (Figure 7f), with a generally stronger and more extensive westward current in the Halo in 2014, when the westward flow extends further northward and reaches the top of Maud Rise at depths below the eastward retroflection current. The zonal flow above and onshore of the Rise also increases between 2009 and 2014.

The zonal flow (Figures 7e and 7f) denotes that a major change in the circulation pattern has occurred between 2009 and 2014 in Maud36. To identify the spatial pattern of this change, it is instructive to examine the relative vorticity of the sea ice (Figure 8). It was shown by Lindsay et al. (2008) that the Halo manifests itself as a band of positive sea-ice vorticity that reflects the anticyclonic oceanic flow around Maud Rise, as previously discussed by Holland (2001). In 2009, a band of strongly positive sea-ice vorticity is found above the Halo, while over the Taylor Cap smaller negative values occur. In between the Halo and the Cap, the retroflection current results in a band of negative vorticity, indicative of cyclonic oceanic flow. In 2014, the positive vorticity signal above the Halo becomes wider and weaker, and its inner flank extends southward into the region in which previously the retroflection current had been present. The retroflection's vorticity signal is now absent. Above the Taylor Cap, small patches of positive and negative vorticity are present, suggesting a more dynamic, eddy-richer water column, as was previously indicated by the zonal velocity (Figure 7f). Thus, overall, the entire Maud Rise region is characterized by more turbulent circulation patterns in 2014 than in 2009.

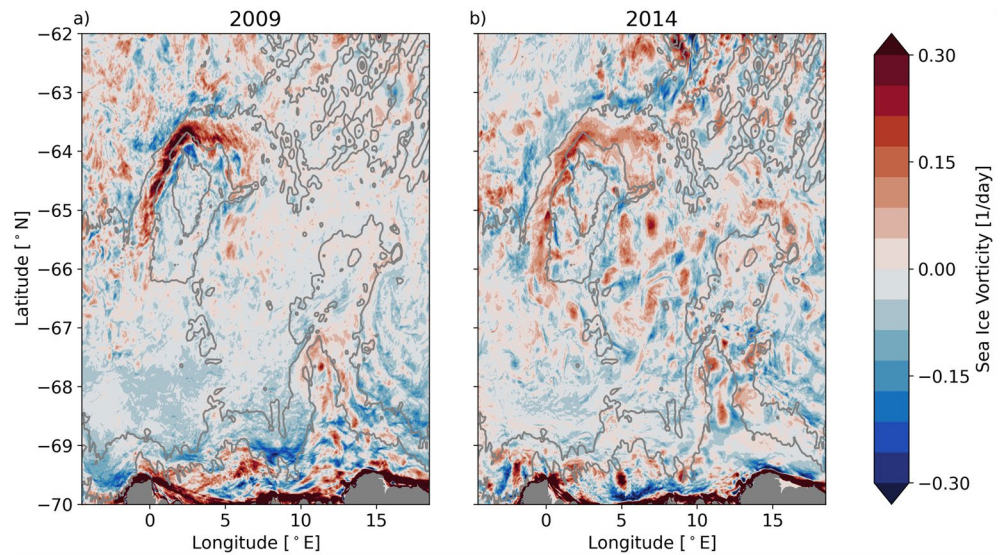


**Figure 8.** Time-mean sea-ice relative vorticity for (a) 2009 and (b) 2014 in Maud36.

### 3.3. Remote Control of Maud Rise Variability

The Halo leaves an imprint on the sea surface height (SSH) structure (Figure 9), being associated with elevated SSH (white dashed line). This imprint does not fully encircle Maud Rise, consistent with the Halo's position found in the in situ observations (Figure 3) and the positive sea-ice vorticity (Figure 8). The hook-shaped feature of elevated SSH implies, via geostrophy, a retroflexion of the water masses along the inner flank of the Halo. Floats have indeed been shown to follow this inner retroflexion path (Mohrmann et al., 2022).

To demonstrate that water from the Halo enters the Taylor Cap through the retroflexion, we correlate  $\sigma_0$  of the subsurface layer (200–1,000 m; Figure 10a) with a reference time series in the western part of the Halo (yellow star in Figure 10a). The water mass found in the western part of the Halo is readily connected to/dependent on the waters upstream, on the northern flank of Maud Rise, over the Astrid Ridge (orange star) and, ultimately, the inflow to the region from the east via the Weddell Gyre (blue star). These dependencies are illustrated by the time series of  $\sigma_0$  (Figure 10b), where the density of the subsurface layer is set by the water mass entering the region in the east (blue line). From there density signals propagate onto the Astrid Ridge (orange line) and into the Halo (red, black and yellow lines). Then, the signals appear also in the Taylor Cap, albeit weaker and with a time lag of 1 year relative to entry to the region (Figure 10a, blue star) or half a year relative to the western part of the Halo (yellow star). The latter lag is as observed for temperature in the upper 1,300 m (Figure 6).

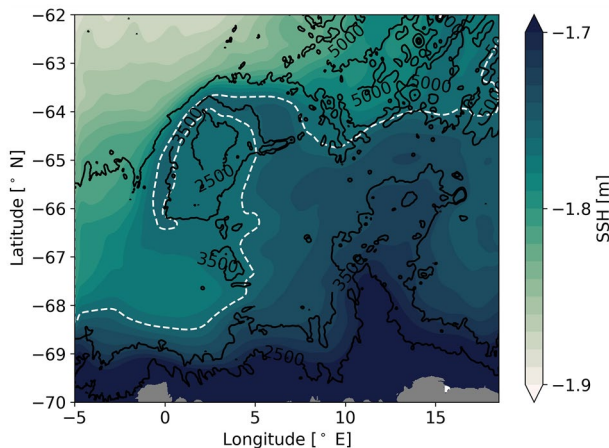


**Figure 9.** Mean SSH in the period 2007–2017 in Maud36. The white dashed contour delineates the  $-1.76$  m SSH signature of the Halo.

The SSH structure and the correlation diagnostics point to a dynamical relation between the Taylor Cap and the Halo. We use the heat budget of the Taylor Cap to assess whether the changes seen therein result from mean advection, eddy transport and/or surface forcing (Figure 11). We have separated the waters in the Taylor Cap into three layers: surface ( $<200$  m), subsurface (200–1,000 m) and deep ( $>1,000$  m). The budget of each layer is sustained by vertical and lateral fluxes (Figures 11a and 11b).

The surface layer's heat budget entails a balance between the surface flux,  $Q_{net}$ , the vertical advective heat flux through a depth of 200 m, and the lateral heat flux. The largest term in this layer is the surface forcing  $Q_{net}$  ( $\pm 1.5 \cdot 10^{12}$  W), which exhibits a prominent seasonal cycle that leaves a strong imprint on the upper-ocean heat content (Figure 11c, yellow line). The other heat flux terms are comparably small, with the exception of the deep convection event in 2007, when the vertical heat flux through 200 m increases to  $10^{12}$  W.



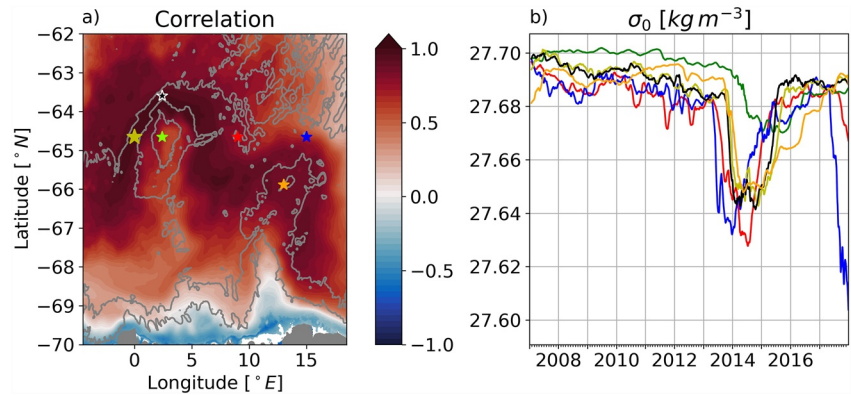


**Figure 10.** (a) Correlation between the average  $\sigma_0$  of the subsurface layer (200–1,000 m) and the  $\sigma_0$  at the location indicated by the yellow star. (b) Time series of the mean  $\sigma_0$  of the subsurface layer with a moving average of 50 days; colors refer to the locations indicated in (a).

The heat budget of the subsurface layer is controlled by the vertical heat fluxes through 200 and 1,000 m and by the lateral heat flux. The vertical heat fluxes through 200 m range from  $-1 \cdot 10^{11}$  to  $0.5 \cdot 10^{11}$  W, and those through 1,000 m range from  $-1.5 \cdot 10^{11}$  to  $0.5 \cdot 10^{11}$  W. The largest fluxes through 200 m occur when the MLD reaches or exceeds 200 m (Figure 11d). Further, large vertical heat fluxes through 200 and 1,000 m are found in 2014, although the maximum MLD is shallower than 200 m. This is linked to the advection of anomalous deep water in the Halo and its retroreflection into the Taylor Cap (Figure 6). The lateral heat fluxes into the layer are always positive and in the range  $0 \cdot 10^{11}$  to  $3 \cdot 10^{11}$  W. This explains the layer's increasing heat content (Figure 11c, blue line). The eddy component of the lateral fluxes (dashed blue line) is of similar magnitude to that

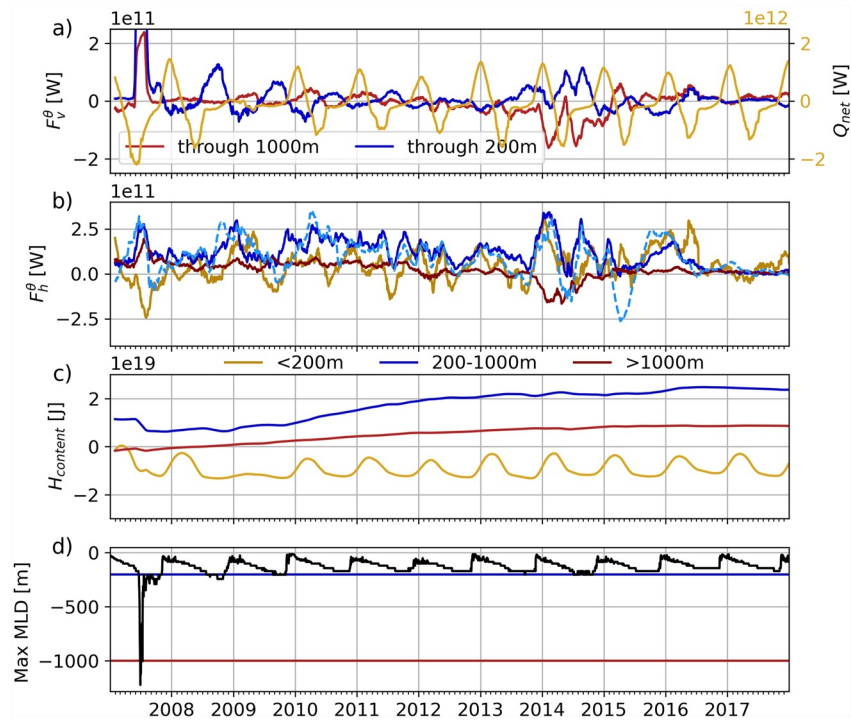


**Figure 11.** Terms of the heat budget for the Taylor Cap in Maud36. (a) Vertical component (defined as upward) of the advective heat flux (Equation 2) at depths of 200 m (blue line) and 1,000 m (red line), and surface heat flux  $Q_{net}$  (yellow line, right y-axis). (b) Horizontal component of the advective heat flux (Equation 2) across the boundaries of the layer volumes (solid lines), and eddy component for the subsurface layer (dashed blue line). Both heat fluxes are defined as positive into the volume. (c) Heat content of the upper 200 m (yellow line), 200–1,000 m (blue line), and below 1,000 m (red line) in the Taylor Cap. (d) Maximum MLD in the Taylor Cap; horizontal lines indicate the boundaries of the subsurface layer.



of the full lateral heat fluxes; thus, the main process governing the warming of the Taylor Cap is the eddy heat flux. Contrary to the full lateral heat fluxes, the eddy heat fluxes induce a heat loss in some periods, especially when the anomalously cold and fresh deep waters are advected in 2014. The changes in the heat content align with the development of the  $T_{\max}$  (Figure 4), as expected.

Similarly to the subsurface layer, the heat content of the deep layer increases over time, with the vertical fluxes being smaller than the lateral ones. The largest vertical and lateral heat fluxes are found during deep convection events, and in 2014. In this year, larger negative lateral heat fluxes occur, related to the increased westward flow below the retroflection current at the northern flank of Maud Rise (Figure 7). The heat budget analysis shows that the properties of the Taylor Cap are closely coupled to the dynamics and heat fluxes in its vicinity, and therefore we find that the Taylor Cap has a limited ability to retain its properties on timescales longer than a few months.

In summary, the heat budget of the three layers shows that the heat content in the upper 200 m of the Taylor Cap is primarily controlled by surface fluxes, while that in the deeper water column is mainly governed by lateral advection by eddies. An exception to this general pattern occurs during deep convection, when the vertical fluxes prevail over the horizontal advection to induce a cooling of the water column.

#### 4. Discussion and Conclusion

Observations in the region around Maud Rise reveal that the warm-water Halo and the Taylor Cap experience large interannual variability of their deep properties. Temperature transects across the warm-water Halo show that the deep properties therein change substantially between 2013 and 2022 (Figure 2). The  $T_{\max}$  of the Halo and Taylor Cap varies on an interannual timescale during our study period of 2007–2022 (Figures 4a and 4b). The  $T_{\max}$  in the Halo is in the range between 0.1°C and 1.3°C, with most profiles exceeding 1.0°C. Changes of  $T_{\max}$  in the Taylor Cap are more pronounced. Here, a  $T_{\max}$  of 0.8°C occurs in 2015, the year preceding the polynya openings of 2016 and 2017. Temperatures as high as 0.7°C and above were not observed in the Taylor Cap in any of the previous field campaigns by Gordon and Huber (1990), Muench et al. (2001), and De Steur et al. (2007). Further, a Taylor Cap with warmer  $T_{\max}$  than that of the Halo, as briefly observed in 2014, was described here for the first time. This result appears robust to a common limitation of Lagrangian platforms in the Southern Ocean: the uncertainty in the position of the platform during sea ice-covered periods. The warm  $T_{\max}$  events in the Taylor Cap in 2015 were measured by two Argo floats. One crossed the region in May 2015, and had accurate positioning. This float showed a temperature increase toward the western edge of the Taylor Cap. The second float communicated its last position before sea-ice cover just south of the Taylor Cap, and surfaced in the north of the Cap 8 months later. Although the  $T_{\max}$  reported by this float was unexpectedly warm during those months, the MLD measured by the float exceeded >100 m, as is characteristic of the Taylor Cap. Thus, while the float's position is not known precisely, it is highly likely that the float traveled over the Taylor Cap or the Cap's western edge while the area was covered by sea ice.

Our observational findings are supported by three different models: a global eddy-permitting reanalysis product (GLORYS12), and two regional ocean configurations with respective horizontal resolutions of 1°/12° (Maud12) and 1°/36° (Maud36). The models broadly endorse observational results related to the evolution of  $T_{\max}$  (Figure 4). Significant inter-model differences emerge in the Taylor Cap, where the observations and GLORYS12 show a cooling during and after the polynya opening, but no cooling or polynya were reproduced in Maud12 and Maud36 (Figure 6). It remains unclear whether the polynya and related deep convection events in GLORYS12 are forced by the data assimilation scheme employed or if they are a consequence of the physically consistent internal variability of the model only. The models indicate that a clear distinction between the Halo and the Taylor Cap in terms of  $T_{\max}$  is not always observed, as the Taylor Cap shows warmer maximum temperatures than the Halo in 2014 (Figures 4c and 5). Our analysis of the Halo-Taylor Cap dynamics in the models shows that the property variability documented here is mostly remotely and occasionally locally driven. The variability of the Halo is remotely driven by advection of deep waters along the eastern limb of the Weddell Gyre. In turn, the variability of the Taylor Cap is governed by eddy transport, which acts to warm the Cap, and by rare events of deep convection, which cool down the Cap (Figures 10 and 11). The eddies responsible for the lateral heat transport into the Taylor Cap follow the retroflection along the Halo's inner flank. Importantly, the residence time in the Taylor Cap is found to be rather short, with a typical 6 month delay between anomalies in the Halo and their advection in the Taylor Cap.

Our results align with the findings of Kurtakoti et al. (2018), who also documented a warming of the subsurface (250–1,000 m) temperature in the years preceding a polynya opening in their climate simulations (their Figure 8). Unlike in our diagnostics, their reported warming did not cause a near-vanishing of the Taylor Cap, but simply a reduced temperature gradient between the Cap and surrounding waters. With our study, we are able to provide observational evidence that these phenomena are an integral part of the regional variability around Maud Rise. Further, we shed light on the eddy transport process mediating the Cap's warming. We show that the near-vanishing of the Taylor Cap is ephemeral and, as illustrated in Figure 4c, the  $T_{\max}$  contrast between the Halo and Taylor Cap grew after 2014, indicating a reappearance of the Cap. Such near-vanishing and reappearance of the Taylor Cap is not incompatible with Kurtakoti et al. (2018), who showed that a stronger Taylor Cap preceded the polynya opening immediately before. Our work indicates that the variability of the Taylor Cap is closely related to the inflow from the Weddell Gyre. A more energized inflow, as found in 2014 (Figure 7f) leads to a shallower MLD (Figure 6d), whereas a slower inflow at other times (e.g., 2009) induces a deeper MLD. This association is in line with the results of Alverson and Owens (1996). The stronger inflow in 2014 may have led to a westward displacement of the Taylor Cap, as suggested by Muench et al. (2001). Another significant finding reported by Kurtakoti et al. (2018) was the advection from Astrid Ridge onto Maud Rise of an upper-ocean (top 100 m) salinity anomaly 1–2 years prior to the polynya opening. We further documented such advected anomalies in the subsurface (200–1,000 m) water masses (Figure 10). Of particular note in our model results was an anomalously cold and fresh subsurface water mass, which originated at a location north of Astrid Ridge. As in the work of Kurtakoti et al. (2018), the anomaly reached Maud Rise along the eastern limb of the Weddell Gyre.

The increased heat content in the Taylor Cap (Figure 11) has an impact on the region's ability to produce deep convection. Persistent changes in advection of warm waters along the flanks of Maud Rise within the Halo are an important preconditioner for the onset of deep convection and the emergence of the polynya (Rheinländer et al., 2021). As such, the representation of the Taylor Cap in models is critical to generate realistic Maud Rise polynyas. The Taylor Cap can only be reproduced correctly if Maud Rise has a realistic height and steepness (Kurtakoti et al., 2018). Results of Neme et al. (2021) (their Figure 7) show that the warm-water Halo is present with 0.1° horizontal resolution. Most of the current ocean and climate models have a coarser resolution, and mainly underestimate the polynya area or do not produce a polynya at all (Mohrman et al., 2021). Our results thus indicate that the mechanisms responsible for the open-ocean ventilation of interior layers might not be correctly represented in these coarser models. However, even with sufficient resolution, models are not guaranteed to produce polynyas as illustrated by our Maud12 and Maud36 simulations. A more targeted tuning of the model and inclusion of thermobaric and cabbeling effects below the mixed layer (Akitomo, 2006; Harcourt, 2005) might be important to increase model realism.

Our analysis suggests that the local surface forcing alone cannot explain why the polynya opened in 2016 and 2017, contrary to previous suggestions (Francis et al., 2020); a preconditioning of the ocean by advection of anomalous deep waters into the region is important. Remotely advected density anomalies in the Weddell Gyre play an important role in determining the vertical stability of the water column around Maud Rise. Our analysis is broadly consistent with the work of Kurtakoti et al. (2021), who suggested that the advection of high surface salinity anomalies from the Astrid Ridge was a key process for polynya formation, based on an eddy-permitting coupled climate simulation. However, the decisive process triggering deep convection and initiating the polynya opening has not been discussed in this work. More localized processes might provide such a trigger, possibly involving submesoscale variability and current-topography interactions.

Our model analysis has also revealed that the properties around Maud Rise were strongly perturbed in 2013 and 2014, leading to the near-vanishing of both the Halo and the Taylor Cap (Figure 7). The origin of this anomaly remains unclear, and it is outside the scope of this study, but it is likely to be associated with the variability in strength of the Weddell Gyre. The latter has been suggestively connected to large-scale climate modes of variability, such as the El Niño-Southern Oscillation (Martinson & Iannuzzi, 2003) or the Southern Annular Mode (Gordon et al., 2007), thus raising the possibility that these climate modes are indirectly responsible for the opening of the polynya. Our work provides new insights into the highly dynamic nature of the local circulation around Maud Rise (including the remotely controlled warm-water Halo and the retroreflection circling around the Taylor Cap) and its role in controlling the area's stratification, heat content and propensity to polynya openings. Further progress will require a continued program of observations in the region, helping to decide whether the observed anomaly in 2013 and 2014 in the Maud Rise leading to the 2016/2017 polynya openings was part of the

system's natural variability, or if it was an indication of the deeper climate changes currently at play (De Lavergne et al., 2014).

## Data Availability Statement

The EN4.2.2 data set (Met Office Hadley Centre, 2022) is available from Met Office Hadley Center at <https://www.metoffice.gov.uk/hadobs/en4/>. The marine mammal data (Marine Mammals Exploring the Oceans Pole to Pole, 2022) were collected and made freely available by the International MEOP Consortium and the national programs that contribute to it (<http://www.meop.net>). The GLORYS12V1 data set (Copernicus Marine Environment Monitoring Service, 2022) is available from Copernicus Marine Environment Monitoring Service (CMEMS) at <https://doi.org/10.48670/moi-00021>. Model parameters used to generate the model output and computer code to reproduce the plotted figures are available in an open-access repository (Gülk, 2023). The SO-CHIC CTD data (Steiger et al., 2022) can be found at <https://doi.org/10.17882/95314>.

## Acknowledgments

The authors thank the three anonymous reviewers and the editor for their useful comments and suggestions. BG, FR, ANG, AN and GM acknowledge support from European Union's Horizon 2020 research and innovation programme under grant agreement No. 821001 (SO-CHIC). We highly appreciate the work of the scientific personal and the ship crew on the SO-CHIC cruise on SA Agulhas II, especially Brian Ward, Nadine Steiger and Jean-Baptiste Sallée. Further, we are grateful for the stimulating discussions with the SO-CHIC team. The computations were enabled by resources provided by the Swedish National Infrastructure for Computing (SNIC) at Tetralith partially funded by the Swedish Research Council through Grant Agreement 2018-05973.

## References

- Akitomo, K. (2006). Thermobaric deep convection, baroclinic instability, and their roles in vertical heat transport around Maud rise in the Weddell Sea. *Journal of Geophysical Research*, 111(C9), C09027. <https://doi.org/10.1029/2005jc003284>
- Alverson, K., & Owens, W. B. (1996). Topographic preconditioning of open-ocean deep convection. *Journal of Physical Oceanography*, 26(10), 2196–2213. [https://doi.org/10.1175/1520-0485\(1996\)026<2196:tpood>2.0.co;2](https://doi.org/10.1175/1520-0485(1996)026<2196:tpood>2.0.co;2)
- Campbell, E. C., Wilson, E. A., Moore, G. K., Riser, S. C., Brayton, C. E., Mazloff, M. R., & Talley, L. D. (2019). Antarctic offshore polynyas linked to southern hemisphere climate anomalies. *Nature*, 570(7761), 319–325. <https://doi.org/10.1038/s41586-019-1294-0>
- Chapman, D. C., & Haidvogel, D. B. (1992). Formation of Taylor Caps over a tall isolated seamount in a stratified ocean. *Geophysical and Astrophysical Fluid Dynamics*, 64(1–4), 31–65. <https://doi.org/10.1080/03091929208228084>
- Cheon, W. G., & Gordon, A. L. (2019). Open-ocean polynyas and deep convection in the southern ocean. *Scientific Reports*, 9(1), 1–9. <https://doi.org/10.1038/s41598-019-43466-2>
- Cisewski, B., Strass, V. H., & Leach, H. (2011). Circulation and transport of water masses in the Lazarev Sea, Antarctica, during summer and winter 2006. *Deep Sea Research Part I: Oceanographic Research Papers*, 58(2), 186–199. <https://doi.org/10.1016/j.dsr.2010.12.001>
- Comiso, J., & Gordon, A. (1987). Recurring polynyas over the Cosmonaut Sea and the Maud rise. *Journal of Geophysical Research*, 92(C3), 2819–2833. <https://doi.org/10.1029/jc092ic03p02819>
- Copernicus Marine Environment Monitoring Service. (2022). Global ocean physics reanalysis. [Dataset]. <https://doi.org/10.48670/moi-00021>
- De Lavergne, C., Paltter, J. B., Galbraith, E. D., Bernardello, R., & Marinov, I. (2014). Cessation of deep convection in the open southern ocean under anthropogenic climate change. *Nature Climate Change*, 4(4), 278–282. <https://doi.org/10.1038/nclimate2132>
- De Steur, L., Holland, D., Muench, R., & McPhee, M. G. (2007). The warm-water “Halo” around Maud Rise: Properties, dynamics and impact. *Deep Sea Research Part I: Oceanographic Research Papers*, 54(6), 871–896. <https://doi.org/10.1016/j.dsr.2007.03.009>
- Francis, D., Mattingly, K. S., Temimi, M., Massom, R., & Heil, P. (2020). On the crucial role of atmospheric rivers in the two major Weddell Polynya Events in 1973 and 2017 in Antarctica. *Science Advances*, 6(46), eabc2695. <https://doi.org/10.1126/sciadv.abc2695>
- GEBCO Compilation Group. (2022). Gebco 2022 grid. <https://doi.org/10.5285/e0f0bb80-ab44-2739-e053-6c86abc0289c>
- Good, S. A., Martin, M. J., & Rayner, N. A. (2013). EN4: Quality controlled ocean temperature and salinity profiles and monthly objective analyses with uncertainty estimates. *Journal of Geophysical Research: Oceans*, 118(12), 6704–6716. <https://doi.org/10.1002/2013jc009067>
- Gordon, A. L. (1982). Weddell deep water variability. *Journal of Marine Research*, 40, 199–217.
- Gordon, A. L., & Huber, B. A. (1990). Southern ocean winter mixed layer. *Journal of Geophysical Research*, 95(C7), 11655–11672. <https://doi.org/10.1029/jc095ic07p11655>
- Gordon, A. L., Visbeck, M., & Comiso, J. C. (2007). A possible link between the weddell polynya and the southern annular mode. *Journal of Climate*, 20(11), 2558–2571. <https://doi.org/10.1175/jcli4046.1>
- Gülk, B. (2023). Maud parameters and data analysis. [Software]. Retrieved from [https://github.com/bguelk/JGR\\_2023\\_MaudRise](https://github.com/bguelk/JGR_2023_MaudRise)
- Harcourt, R. R. (2005). Thermobaric cabbelling over Maud Rise: Theory and large eddy simulation. *Progress in Oceanography*, 67(1–2), 186–244. <https://doi.org/10.1016/j.pocean.2004.12.001>
- Holland, D. (2001). Explaining the Weddell Polynya—A large ocean eddy shed at Maud Rise. *Science*, 292(5522), 1697–1700. <https://doi.org/10.1126/science.1059322>
- Kurtakoti, P., Veneziani, M., Stössel, A., & Weijer, W. (2018). Preconditioning and formation of Maud Rise polynyas in a high-resolution Earth system model. *Journal of Climate*, 31(23), 9659–9678. <https://doi.org/10.1175/jcli-d-18-0392.1>
- Kurtakoti, P., Veneziani, M., Stössel, A., Weijer, W., & Maltrud, M. (2021). On the generation of Weddell Sea Polynyas in a high-resolution Earth system model. *Journal of Climate*, 34(7), 2491–2510. <https://doi.org/10.1175/jcli-d-20-0229.1>
- Leach, H., Strass, V., & Cisewski, B. (2011). Modification by lateral mixing of the warm deep water entering the Weddell Sea in the Maud Rise region. *Ocean Dynamics*, 61(1), 51–68. <https://doi.org/10.1007/s10236-010-0342-y>
- Lellouche, J.-M., Greiner, E., Bourdallé-Badie, R., Garric, G., Melet, A., Drévillon, M., et al. (2021). The copernicus global 1/12° oceanic and sea ice GLORYS12 reanalysis. *Frontiers in Earth Science*, 9. <https://doi.org/10.3389/feart.2021.698876>
- Lindsay, R., Kwok, R., De Steur, L., & Meier, W. (2008). Halo of ice deformation observed over the Maud Rise seamount. *Geophysical Research Letters*, 35(15), L15501. <https://doi.org/10.1029/2008gl034629>
- Madec, G., & NEMO System Team. (2019). *NEMO ocean engine*. Scientific Notes of Climate Modelling Center, Institut Pierre-Simon Laplace (IPSL). <https://doi.org/10.5281/ZENODO.1464816>
- Marine Mammals Exploring the Oceans Pole to Pole (2022). Meop [Dataset]. Retrieved from <http://www.meop.net>
- Martinson, D. G. (1990). Evolution of the southern ocean winter mixed layer and sea ice: Open ocean deepwater formation and ventilation. *Journal of Geophysical Research*, 95(C7), 11641–11654. <https://doi.org/10.1029/jc095ic07p11641>
- Martinson, D. G., & Iannuzzi, R. A. (2003). Spatial/temporal patterns in Weddell Gyre characteristics and their relationship to global climate. *Journal of Geophysical Research*, 108(C4), 8083. <https://doi.org/10.1029/2000jc000538>

- McMahon, C. R., Roquet, F., Baudel, S., Belbeoch, M., Bestley, S., Blight, C., et al. (2021). Animal borne ocean sensors—AniBOS—An essential component of the global ocean observing system. *Frontiers in Marine Science*, 1625.
- McPhee, M. G. (2000). Marginal thermobaric stability in the ice-covered upper ocean over Maud Rise. *Journal of Physical Oceanography*, 30(11), 2710–2722. [https://doi.org/10.1175/1520-0485\(2000\)030<2710:mtsiti>2.0.co;2](https://doi.org/10.1175/1520-0485(2000)030<2710:mtsiti>2.0.co;2)
- Met Office Hadley Centre. (2022). En4 quality controlled ocean data [Dataset]. Retrieved from <https://www.metoffice.gov.uk/hadobs/en4/>
- Mohrmann, M., Heuzé, C., & Swart, S. (2021). Southern Ocean Polynyas in CMIP6 models. *The Cryosphere*, 15(9), 4281–4313. <https://doi.org/10.5194/tc-15-4281-2021>
- Mohrmann, M., Swart, S., & Heuzé, C. (2022). Observed mixing at the flanks of Maud Rise in the Weddell Sea. *Geophysical Research Letters*, 49(8), e2022GL098036. <https://doi.org/10.1029/2022gl098036>
- Muench, R., Morison, J., Padman, L., Martinson, D., Schlosser, P., Huber, B., & Hohmann, R. (2001). Maud rise revisited. *Journal of Geophysical Research*, 106(C2), 2423–2440. <https://doi.org/10.1029/2000jc000531>
- Neme, J., England, M. H., & Hogg, A. M. (2021). Seasonal and interannual variability of the Weddell Gyre from a high-resolution global ocean-sea ice simulation during 1958–2018. *Journal of Geophysical Research: Oceans*, 126(11), e2021JC017662. <https://doi.org/10.1029/2021jc017662>
- NEMO Sea Ice Working Group. (2018). *Sea ice modelling integrated initiative (si3) – The nemo sea ice engine (No. 31)*. Zenodo. <https://doi.org/10.5281/zenodo.1471689>
- Proudman, J. (1916). On the motion of solids in a liquid possessing vorticity. *Proceedings of the Royal Society of London - Series A: Containing Papers of a Mathematical and Physical Character*, 92(642), 408–424.
- Reeve, K. A., Boebel, O., Strass, V., Kanzow, T., & Gerdes, R. (2019). Horizontal circulation and volume transports in the Weddell Gyre derived from Argo float data. *Progress in Oceanography*, 175, 263–283. <https://doi.org/10.1016/j.pcean.2019.04.006>
- Rheinländer, J. W., Smedsrud, L. H., & Nisancioglu, K. H. (2021). Internal ocean dynamics control the long-term evolution of Weddell Sea Polynya activity. *Frontiers in Climate*, 3, 718016. <https://doi.org/10.3389/fclim.2021.718016>
- Rodgers, K. B., Aumont, O., Mikaloff Fletcher, S., Plancherel, Y., Bopp, L., de Boyer Montégut, C., et al. (2014). Strong sensitivity of Southern Ocean carbon uptake and nutrient cycling to wind stirring. *Biogeosciences*, 11(15), 4077–4098. <https://doi.org/10.5194/bg-11-4077-2014>
- Ryan, S., Schröder, M., Huhn, O., & Timmermann, R. (2016). On the warm inflow at the eastern boundary of the Weddell Gyre. *Deep Sea Research Part I: Oceanographic Research Papers*, 107, 70–81. <https://doi.org/10.1016/j.dsr.2015.11.002>
- Sallée, J., Abrahamson, E., Allaire, C., Auger, M., Ayres, H., Badhe, R., et al. (2023). Southern ocean carbon and heat impact on climate. *Philosophical Transactions of the Royal Society A*, 381(2249). <https://doi.org/10.1098/rsta.2022.0056>
- Schröder, M., & Fahrback, E. (1999). On the structure and the transport of the eastern Weddell Gyre. *Deep Sea Research Part II: Topical Studies in Oceanography*, 46(1–2), 501–527. [https://doi.org/10.1016/s0967-0645\(98\)00112-x](https://doi.org/10.1016/s0967-0645(98)00112-x)
- Sévellec, F., Naveira Garabato, A., Brearley, J., & Sheen, K. (2015). Vertical flow in the southern ocean estimated from individual moorings. *Journal of Physical Oceanography*, 45(9), 2209–2220. <https://doi.org/10.1175/jpo-d-14-0065.1>
- Steiger, N., Sallée, J., Ward, B., Azevedo, A., Binase, Z., Ten Doeschat, A., et al. (2022). CTD observation - So-Chic Cruise 2022 [Dataset]. SEANOE <https://doi.org/10.17882/95314>
- Taylor, G. I. (1923). Experiments on the motion of solid bodies in rotating fluids. *Proceedings of the Royal Society of London - Series A: Containing Papers of a Mathematical and Physical Character*, 104(725), 213–218.
- Tsujino, H., Urakawa, S., Nakano, H., Small, R. J., Kim, W. M., Yeager, S. G., et al. (2018). JRA-55 based surface dataset for driving ocean-sea-ice models (JRA55-DO). *Ocean Modelling*, 130, 79–139. <https://doi.org/10.1016/j.ocemod.2018.07.002>
- Ward, B., Azevedo, A., Binase, Z., ten Doeschate, A., Els, H., Hamna, S., et al. (2022). *SoChic cruise report*. Zenodo. <https://doi.org/10.5281/zenodo.6948850>